ACTIVE FLOW CONTROL BY THE SLIDING ELECTRIC ARC DISCHARGE

V.S. Aksenov, S.A. Gubin
Moscow Engineering Physics Institute, Russia

D.V. Blagodatskih, M.V. Bragin, V.V. Golub, V.V. Volodin
Institute for High Energy Densities, Russia

I.N. Laskin
Central Institute for Aviation Motors, Russia

Introduction

In the aerodynamic configuration design of hypersonic vehicles it should be provided maximum of total pressure recovery coefficient and flow uniformity at the air-breather inlet at minimal drag force.

As usual the maintaining of required air compression achieving with the head part shape choice, also shape may be changed by "heat action".

It was shown in [1,2] that the bulk thermal energy supply in the flow upstream the scramjet intake allows to reduce drag force and increase the total pressure recovery coefficient. Obvious disadvantages of such heat supply are difficulties of practical realization and decrease of air mass flow through the air-breather.

Usual way of the air mass flow through the intake increase is application of additional sidepieces for air flow confinement and prevention air flow spreading upstream the inlet. This leads to the significant drag force increase. Sidepieces at the bottom of hypersonic flying vehicle head part may be reduced or replaced with the thermal energy release as heat lines on the vehicle surface.

It is necessary to provide heat supply not in the air flow that come to the intake, but provide the "effective shape correction" with heat supply without deterioration of intake characteristics.

In the paper new combined approach of the hypersonic vehicle flow enhancement using the thermal energy release as heat lines induced by electric arc discharge is proposed.

Sliding electric arc discharge as a mean of the aircraft trajectory control has been proposed in [3]. The electric discharge sliding from one electrode to another on a semiconducting surface and terminating by arc discharge generating a shock wave in the surrounding air. A shock wave generating by sliding electric arc discharge at the aircraft surface modifies the character of the surface flow and produces force to aircraft trajectory control.

A material at the surface of which the discharge is generated may be carbon, carbon-containing ceramics and some other semiconductors has been shown in [3].

Experimental Installation and Numerical Method

The excitation of discharge was realized by the breakdown of spark gaps between electrodes and the surface of a semiconductor graphite rod located in measuring section of low-pressure chamber perpendicular and in the direction of shock tube axis. The discharge gap was situated "flush" to the lower part of measuring section perpendicular or in the direction of shock tube axis.

The evolution of electric discharge in high speed flow behind the shock wave was imaged by the shadow and interference photography techniques using a system consisted of an IAB-458 shadow device, an optical interference device and SFR high-speed camera. Modified OGM-20 ruby laser had been used as the light source.

In the numerical part of investigation intake flow and drag force characteristics at the hypersonic vehicle were estimated.

Parabolized Navier-Stokes equations system was used for the flow simulation. Effectiveness of the system concerned the fact of in the case of inviscid steady supersonic flows with dominant direction 3D flows simulation come to 2D task solution with effective explicit scheme application. Restriction on the longitudinal step is dictated by the task physics. Number of dimensions reduction is the favorable factor having the crucial sense in the most of the cases. So the simulation of inviscid steady supersonic flows with dominant direction in complex configurations may be carried out more fast, easy and accurate with spatial march approach. Development of such approach with the taking into account of local subsonic regions namely boundary layers yielded so called "parabolized" branch of computational fluid dynamics. Parabolized system contains all components of Euler's equations and boundary layer equations. Hence it allows to describe supersonic regions of inviscid flow and boundary

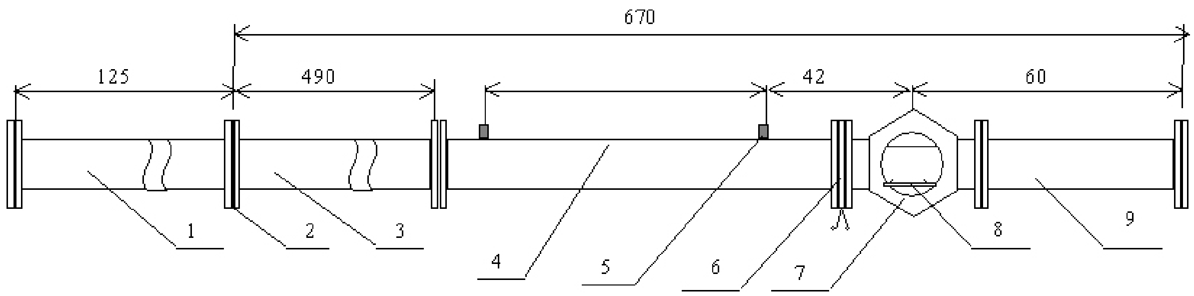

Fig. 1. *1* – high pressure chamber, *2* –diaphragm, *3* – low pressure chamber, *4* – control section, *5* – pressure gauge, *6* – dielectric section, *7* – visualization section, *8* – discharge gap, *9* – end section.The interelectrode gap width was equal to 60 mm. The storage bank with a capacitance of 50 mkF was used. The initial voltage was varied in the range from 2.6 to 3.35 kV. The low-pressure chamber was filled with air at initial pressures of 0.09 – 1 atm. The experimental installation schematic is presented in Figs.1, 2

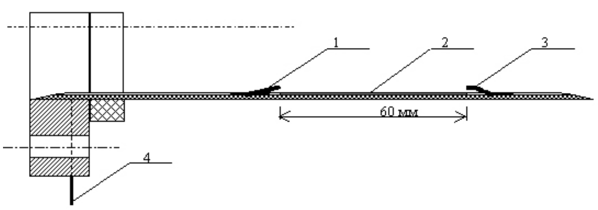

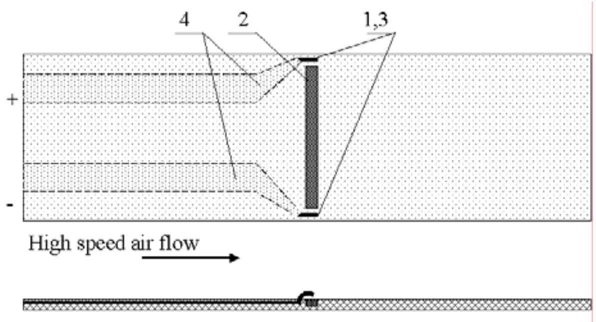

Fig. 2. Discharge gap arrangement along the flow (top), across the flow (bottom) *1* –negative electrode, *2* – semiconductor rod, *3* – positive electrode, *4* –electrodes output

layers with some simple procedures. This system is obtained from the full Navier-Stokes system by the truncation of the components responsible for the diffusive transport along the march direction. As the *X* coordinate (dominant direction) flow direction is choosing.

Integral conservation laws in Decart coordinate system will be:

$$\iint\left(\vec{\mathbf{E}}dydz + \left(\vec{\mathbf{F}} + \vec{\mathbf{F}}_V\right)dxdz + \left(\vec{\mathbf{G}} + \vec{\mathbf{G}}_V\right)dxdy\right) = 0$$

Integration is carrying out on the surface of the volume under consideration. Vectors **E**, **F** and **G** correspond Euler's equations, vectors $\mathbf{F}_v$, and $\mathbf{G}_v$ describe viscous tensions:

$$\vec{\mathbf{E}} = \begin{bmatrix} \rho u \\ \rho u^2 + P \\ \rho uv \\ \rho uw \\ \rho u\left(h + V^2/2\right) \end{bmatrix}; \quad \vec{\mathbf{F}} = \begin{bmatrix} \rho v \\ \rho uv \\ \rho v^2 + P \\ \rho vw \\ \rho v\left(h + V^2/2\right) \end{bmatrix};$$

$$\vec{\mathbf{G}} = \begin{bmatrix} \rho w \\ \rho uw \\ \rho vw \\ \rho w^2 + P \\ \rho w\left(h + V^2/2\right) \end{bmatrix}; \quad \vec{\mathbf{F}}_v = \begin{bmatrix} 0 \\ \sigma_{yx} \\ \sigma_{yy} \\ \sigma_{yz} \\ q_y \end{bmatrix}; \quad \vec{\mathbf{G}}_v = \begin{bmatrix} 0 \\ \sigma_{zx} \\ \sigma_{zy} \\ \sigma_{zz} \\ q_z \end{bmatrix},$$

here u, v, w – components of velocity vector $\vec{\mathbf{V}}$ along the coordinate axes x, y, z, V – velocity vector module, ρ – density, P – pressure, h – specific enthalpy. Here μ is responsible for dynamic viscosity coefficient, Pr – Prandtl number, Re – Reynolds number. $\vec{\mathbf{F}}_v$ and $\vec{\mathbf{G}}_v$ vectors of viscous tenses are of next form:

$$\sigma_{yx} = -\mu\frac{\partial u}{\partial y};$$

$$\sigma_{yy} = -2\mu\frac{\partial v}{\partial y} + \mu'\left(\frac{\partial v}{\partial y} + \frac{\partial w}{\partial z}\right);$$

$$\sigma_{yz} = -\mu\left(\frac{\partial v}{\partial z} + \frac{\partial w}{\partial y}\right);.$$

$$\sigma_{zx} = -\mu\frac{\partial u}{\partial z};$$

$$\sigma_{zy} = -\mu\left(\frac{\partial w}{\partial y} + \frac{\partial v}{\partial z}\right); \quad ,$$

$$\sigma_{zz} = -2\mu\frac{\partial w}{\partial z} + \mu'\left(\frac{\partial v}{\partial y} + \frac{\partial w}{\partial z}\right).$$

In the presented relationships $\mu' = 2\mu/3$, second viscosity is supposed to be zero. System contains five scalar conservation laws and binds six values under consideration (three components of velocity vector, density, pressure and intrinsic energy). For the system closing it is necessary to use the equation of thermodynamic gas properties – equation of state. Gas considered to be ideal and obeys Klapeyron's law: $P = \rho RT$ (R – gas constant, T – temperature).

System under consideration is *X*-hyperbolic-parabolic only in the case of supersonic longitudinal velocity component. It allows march computation from section to section (along X coordinate) downstream. Presence of subsonic regions in the flow requires special regulating procedures. Most using approach is the second component of **E** vector presenting as $\mathbf{E}_2 = \rho u^2 + \omega p$, where ω - some function of local Mach number calculated from longitudinal velocity component ($M_x = u/c$, c – sonic velocity). Choice of $\omega = (M_x)^2$ in subsonic ($\omega \equiv 1$ in the case of $M_x > 1$) regions provides march calculation stability.

Results

Figures 3, 5 and 7 illustrate the development of sliding electric arc discharge in the flow behind the front of a shock wave formed in air at initial pressure $P_0 = 1.0$, 0.25, 1.0 atm and shock wave velocity 560, 721, 577 m/s (Mach number M_0=1.63, 2.1, 1.7), respectively. In these cases the initiation voltage U_0 was equal to 2.5, 2.6, 2.0 kV, respectively. Discharger was arranged across the shock tube axis.

Cinegramms on Fig. 3 and Fig. 5. show the stable development of sliding electric arc discharge in the flow behind the front of a shock wave. The high-velocity air flow under some conditions does not significantly influence to closure of the discharge gap but distorts the form of energy-release area. On Fig. 5 is shown plasma cord was blown off by air flow. The arc is distorted in transverse air flow extending in its direction. However, sliding electric arc discharge is stable developed in these conditions.

The comparison of cinegramms, made in condition rest-air and high speed air flow, shows that main difference is concluded in distortion usually symmetrical and close to cylindrical form of the shock wave front, generated by linear discharge, and the drift of the front and plasma cloud downstream on the air flow.

Cinegramm on Fig. 7 illustrates development of plasma formation in critical condition, when does not occur closing an electrode by plasma contact. Plasma cord was blown off by air flow and did not arrive opposite contact. Electrical arc of short circuit was not generated in this case.

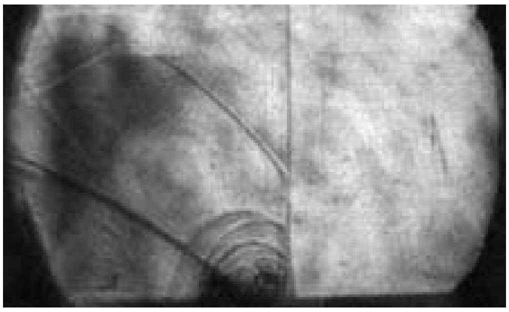

Frame 1

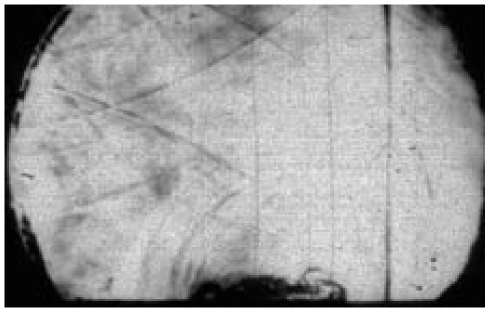

Frame 2

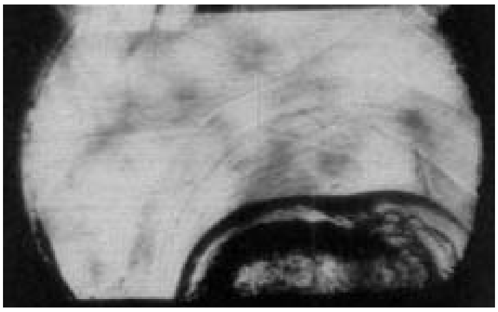

Frame 3

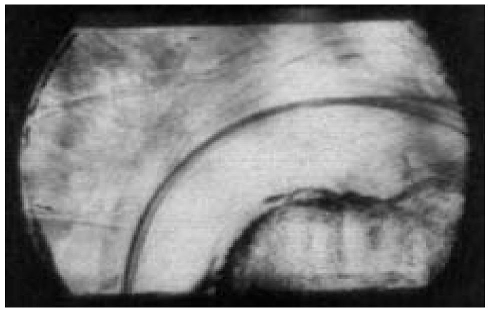

Frame 4

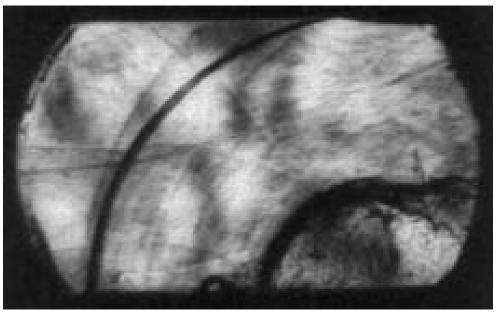

Frame 5

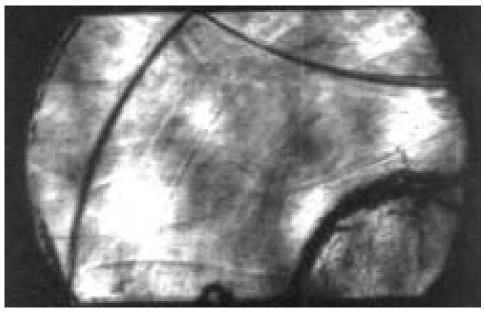

Frame 6

Direction of the air flow left to right.
Direction of the current is perpendicular to the picture plane and the air flow.

Fig.3. The stable development of sliding electric arc discharge behind the front of a shock wave formed in air (P_0=1.0 atm, M_0=1.63)

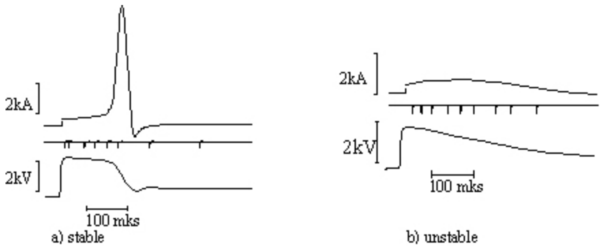

Fig.4. Current and pressure time histories in the cases of stable (a) and unstable (b) sliding discharge formation

Fig.4a) illustrates the stable initiation of sliding electric arc discharge. The current measurements and frame recording of the process have shown that the time of stable electric arc discharge development can be subdivided into two successive stages. The first is the initiation and propagation of streamer from one electrode to another. The second is the shortening of the spark gap by plasma channel and the development of arc discharge. In the first stage the initial current determined by the rod conductivity and the given initial voltage U_0 increases as the discharge front slides along the rod reaching the value of ~$1.5–2 \cdot I_0$. The drastic current increase and fall of the voltage are caused by arc forming when closing electrode by plasma cord occurs in the second stage. The main part of spark energy is released in the arc discharge stage. The released energy forms intense cylindrical compression wave.

The main feature of sliding discharge is a gap which is wider in 1–2 orders of magnitude than that in the air. It results in greater part of electric energy transition into shock wave due to the involvement of greater mass of air into plasma discharge cord forming compared to an ordinary spark discharge.

Fig. 4b) illustrates the unstable initiation of sliding electric arc discharge. In case of unstable initiation of discharge the current and voltage evolution occurs smoothly without drastic change. Since the stage of the electric arc forming is absent and plasma cord does not reach one another. Electrical arc is not generated in this case and discharge energy

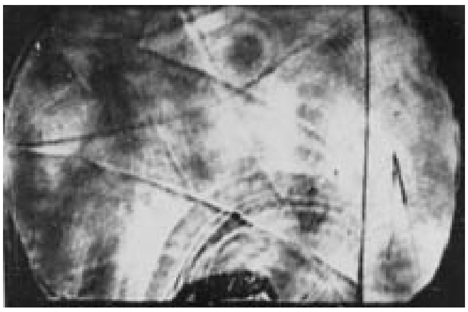

Frame 1

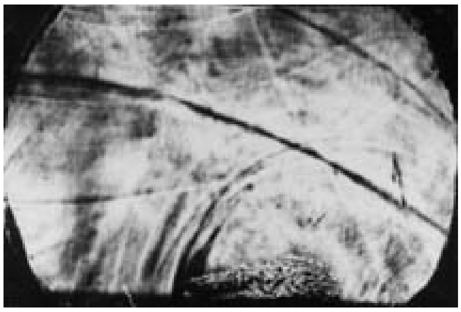

Frame 2

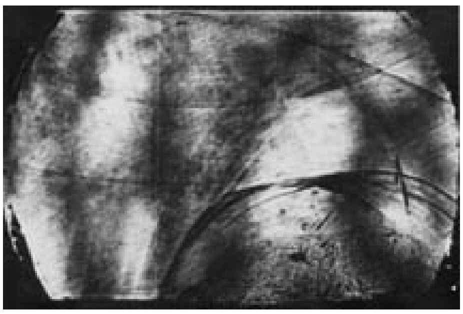

Frame 3

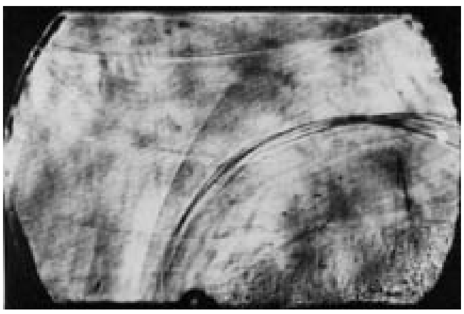

Frame 4

Direction of the air flow left to right.
Direction of the current is perpendicular to the picture plane and the air flow.

Fig. 5. The stable development of sliding electric arc discharge behind the front of a shock wave formed in air ($P_0 = 0.25$ atm, $M_0 = 2.1$)

release time exceeds in 5 times and more the stable regime discharge time.

Critical conditions of sliding electric arc discharge initiation on the flow Mach number at the discharge gap across and along the flow are presented in Fig.6.

Head part configuration is new experimental configuration developed in CIAM (Fig. 8). Bottom surface is two-step wedge with the angles of 3.5° and 7.38°. Length of first step is 2.1 m. Whole length of head part is equal to 3.48 m. Flight Mach number was equal to 7, attack angle was equal to 4°.

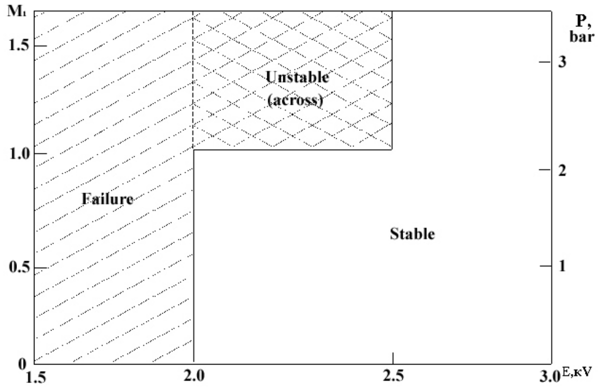

Fig. 6. Critical conditions of sliding electric arc discharge initiation

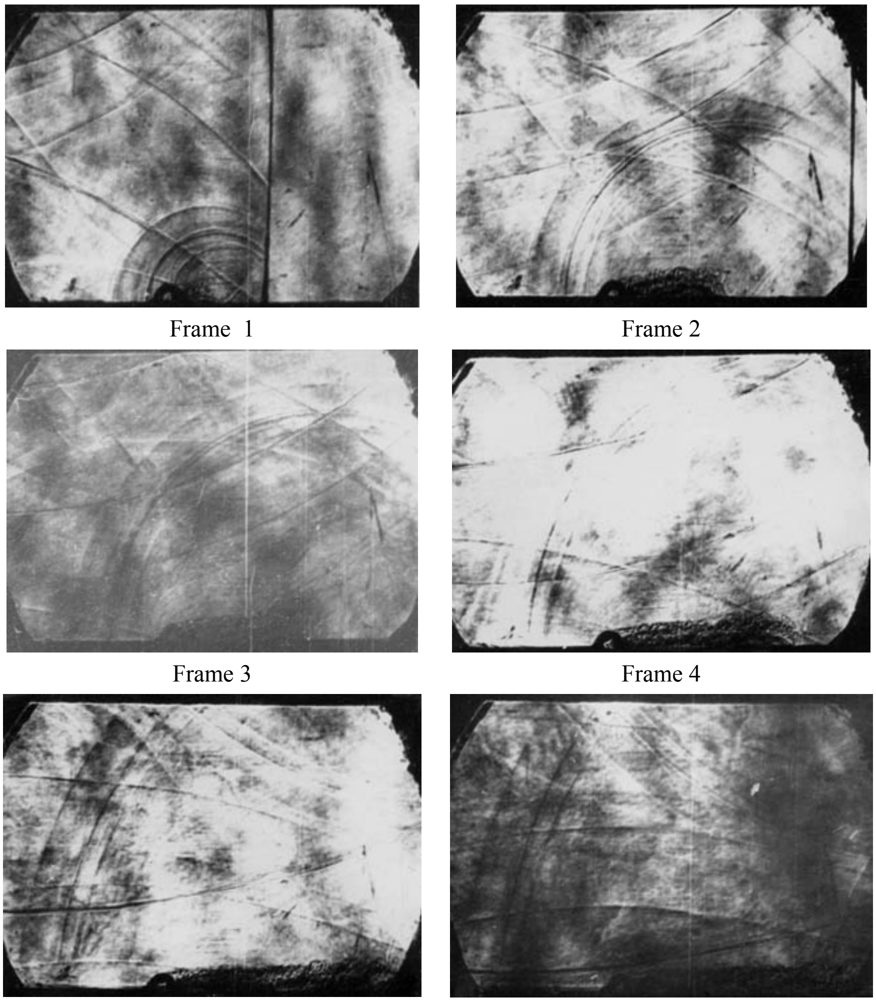

Frame 1 Frame 2

Frame 3 Frame 4

Frame 5 Frame 6

Direction of the air flow left to right
Direction of the current is perpendicular to the picture plane and the air flow

Fig. 7. The unstable development of sliding electric arc discharge behind the front of a shock wave formed in air (P_0 = 1.0 atm, M_0 = 1.7)

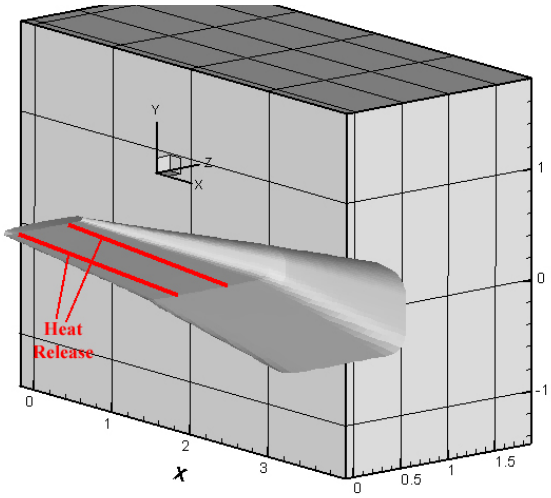

Fig. 8. Head part with heat release regions

Heat is suggested to be releasing in the two linear regions on the vehicle head part provide the effect on the airflow incoming to the air-breather same as additional sidepieces. This prevents the flow diffluence and provides air pressure and mass flow higher than without intake flow additional control. “Heat action” changes the effective shape of vehicle head part. In the simulation heat of 2% from total flow enthalpy releases in two linear regions on the head part bottom surface were considered. Regions were arranged parallel to the flow.

Table 1

Gas parameters at the air-breather enter without and with heat release (HR)

	w/o HR	with HR
Pressure	7.4	7.54
Total pressure recovery	0.755	0.705
C_x	1.59	1.52

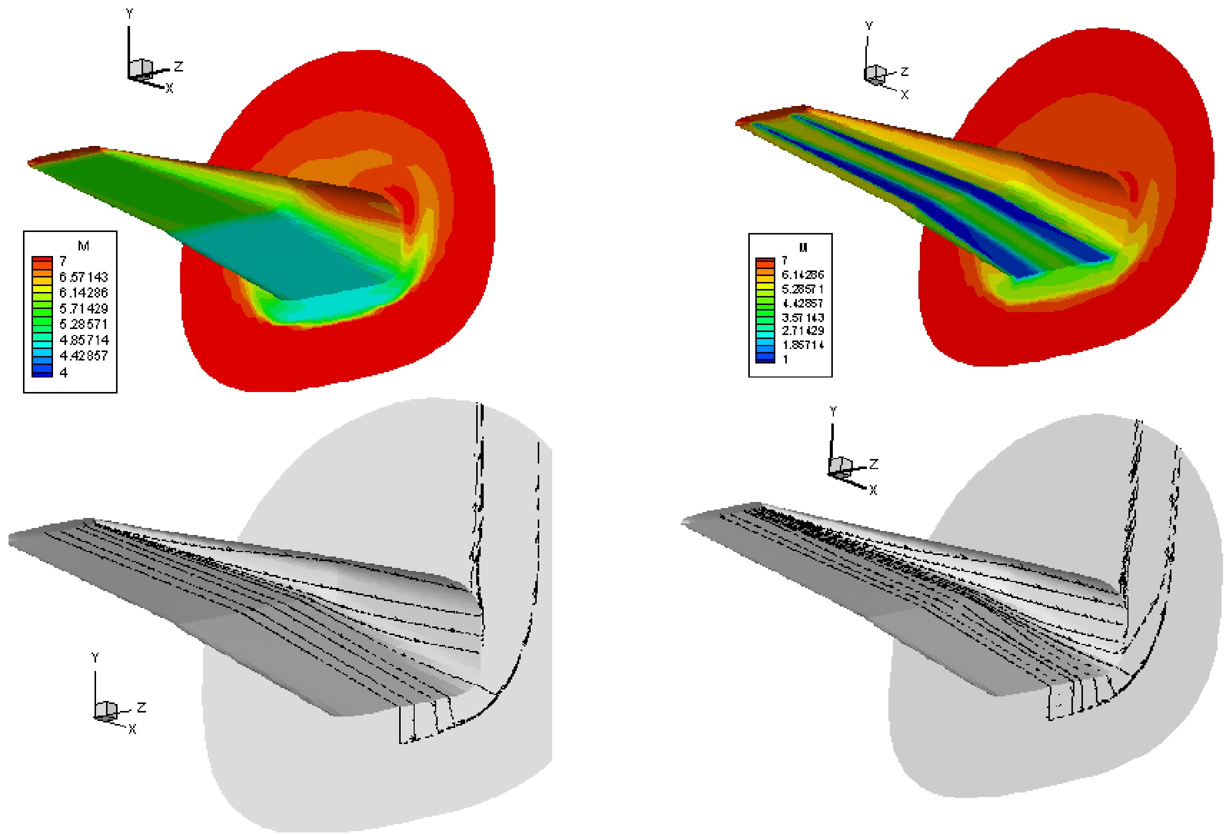

Without heat lines With heat lines

Fig. 9. Results of numerical simulation. Mach numbers distribution (top) and streamlines (bottom) without (left) and with (right) on-body heat release

One can see that in the absence of heat energy release the air-flow is spilling from the head part bottom to the sides and don't reach the air-breather. In the case of heat energy release in the aforementioned regions shock wave configuration preventing the air-flow diffluence is forming on the head part bottom. Air-flow restricted by the heat energy release regions reaches the air-breather (Table 1).

Conclusions

Stable initiation of sliding electric discharge was observed at initiation voltage U0 > 2 kV in the case of discharger arrangement along the shock tube axis in the flow behind the shock waves of Mach numbers ranged from 1.3 to 3.4. In this case the direction of plasma streamer propagation from one electrode to another (streamwise or counter-streamwise) didn't affect on discharge initiation dynamics.

If discharger is arranged across the tube axis the critical regimes of discharge evolution are detected, plasma cord was blown off by air flow and possibly did not arrive opposite electrode.

Stable initiation of sliding electric discharge was observed at initiation voltage $U_0 > 2.5$ kV at all shock wave Mach numbers. Critical conditions of sliding discharge initiation without generation electric arc and without occurrence of shock wave were obtained in the range of initiation voltage 2 kV $< U_0 <$ 2.5 kV and at initial pressures $P_0 \geq 0.5$ atm and shock wave Mach numbers $1.5 < M_0 < 2$. For the initial pressure of shock tube of 0.25 atm unstable discharge at initial voltage of $U_0 = 2.1$ kV and shock wave Mach number of $M_0 \approx 2.8$ was observed. At very strong shock waves ($M > 2.8$) there is stable initiation of sliding electric discharge at initiation voltage of $U_0 < 3.0$ kV.

The most important factor affecting sliding electric discharge is the initial voltage or field strength on discharger.

The second factors are initial pressure and the temperature affecting electric strength of the gas. Reduction of the pressure and increasing of the temperature promote propagation of sliding electric discharge.

The shock wave velocity effect is ambiguous. Increase of shock wave velocity brings on the one hand to increase the pressure and velocities of the flow, and speed force of the dense gas blows off the arc. On the other hand increasing of the temperature of the air flow with increase the shock wave velocity reduces the electric strength of the gas and promotes stability of sliding electric arc discharge.

Thermal energy release makes possible to enhance the intake characteristics (static pressure increase of 2%) at flight Mach number of 7 and the supply of 2% of total flow enthalpy. The head part drag force is reducing for 4.5%.

Acknowledgement

The investigation was partially supported by Presidium of the Russian Academy of Sciences (project N20-2003).

References

[1] T.A. Bormotova, V.V. Golub, V.V. Volodin, I.N. Laskin (2002) The thermal correction of scramjet intake // *In: Proceedings of the 23rd International Symposium on Shock Waves, ed. by F Lu*. Arlington, USA, 2002.

[2] T.A. Bormotova, V.V. Golub, V.V. Volodin, IN Laskin (2003) The Thermal Correction of the Inlet Diffuser of a Hypersonic Scramjet Engine. *High Temperature Vol. 41, No. 3*, 2003 p.415-417

[3] V.S. Aksenov, V.V. Golub, S.A. Gubin, V.P. Efremov, I.V. Maklashova, A.I. Kharitonov and Yu.L. Sharov (2004) Sliding Electric Arc Discharge as a Means of Aircraft Trajectory Control. *Tech. Phys. Letters Vol. 30, No. 10,* 2004:871-873